To Dr. A. Elias, Topical Editor

Each issue has been addressed in the Comment/Response format. These responses were highlighted in bold typeface.

Point-by-point replies to the comments raised by Referee #1 is given below.

Comment 1:

What is new in the current paper and its broad title.

Response:

A paragraph has been added to Section 3 (Lines 75-76, 118-119, 137-153) emphasizing our primary finding that evaporation of ionospheric plasmas into the magnetosphere builds up parallel potentials in higher altitudes by the charge separation of ionospheric plasmas in the mirror geometry. These potentials initiate substorms arising out of arcs and modify existing magnetospheric convection patterns in the equatorial plane.

For the above reason, we prefer to leave unchanged the title “Ionospheric control of space weather”.

Comment 2:

Prior literatures and discussion.

Response:

Abstract (Lines 11-22), Introduction (Lines 26-49), and Summary and Discussion (Lines 189-227) were all revised to include more inclusive reference to past research and discussions.

Point-by-point replies to the comments raised by Referee #2 is given below.

Comment 1:

Electric fields inside the Dipolarization Front.

Response:

Thank you for this information.

Comment 2:

generator

Response:

Explanations are given in Lines 189-197.

Comment 3:

caried -> carried

Response:

Corrected.

Comment 4:

edges of the ionosphere & southward/northward

Response:

Edge of the ionosphere changed to edge of the flow channel, southward/northward to equatorward/poleward. Lines 164-186.

Comment 5:

estimation of upward current density

Response:

New calculations of the field-aligned current density are provided in Lines 165-186.

Comment 6:

extension of ionospheric injection scenario

Response:

We clarified in the introduction that this report is meant to extend the ionospheric injection scenario proposed by Saka (2019) into the magnetosphere region. A new paragraph is added in Section 3 (Lines 75-76, 118-119, 137-153) to explain this enlarged concept.

For more complete explanation, please refer to the Abstract (Lines 11-22), Introduction (Lines 26-49), and Summary and Discussion (Lines 189-227).

Ionospheric control of space weather

Osuke Saka
Office Geophysik, Ogoori, 838-0141, Japan

Abstract

As proposed by Saka (2019), plasma injections arising out of the auroral ionosphere (ionospheric injection) are a characteristic process of the polar ionosphere at substorm onset. The ionospheric injection is triggered by westward electric fields transmitted from the convection surge in the magnetosphere at field line dipolarization. Localized westward electric fields result in local accumulation of ionospheric electrons/ions which produce local electrostatic potentials in the auroral ionosphere. Field-aligned electric fields are developed to extract excess charges from the ionosphere. This process is essential to equipotential equilibrium of the auroral ionosphere. Cold electrons/ions that evaporate from the auroral ionosphere by ionospheric injection tend to generate electrostatic parallel potential below an altitude of 10,000 km. This is a result of charge separation along the mirror fields introduced by the evaporated electrons and ions moving earthward in phase space.

1. Introduction

Discontinuous reconfigurations of geomagnetic fields, referred to as field line dipolarization, are a significant geomagnetic event at substorm onset. Various causes have been suggested, most notably: the formation of X-points [Baker, et al., 1996]; flow braking [Birn et al., 1999]; local enhancement of plasma pressures [Tanaka et al., 2010]; arrival of plasma bubbles [Birn et al., 2004]; plasma instabilities [McPherron et al., 1973; Roux et al., 1991; Lui, 1996; Liu and Liang, 2009]; and relaxation of radial inhomogeneity [Saka, 2020]. Field line dipolarization alters global current circuits in the midnight magnetosphere thereby dipolarizing geomagnetic field lines [McPherron et al., 1973].

Field line dipolarization invokes inductive westward electric fields at the equatorial plane with the arrival of Dipolarization Front [Runov et al., 2011; Liu et al., 2014]. These

fields penetrate the polar ionosphere and yield plasma injections from the ionosphere (ionospheric injection) with associated nonlinear evolution of the plasma motions [Saka, 2019]. This development in turn leads to poleward expansion of auroras [e.g., Nielsen and Greenwald, 1978] and vertical flows of ionospheric plasmas [e.g., Wahlund et al., 1992]. Ionospheric injection can be regarded as an evaporation of ionospheric plasmas into the magnetosphere. This report focuses on how this evaporation process builds up parallel potentials in higher altitudes above the ionosphere to initiate auroral onset.

In Section 2, ionospheric injection scenario associated with field line dipolarization is briefly described. In Section 3, development of parallel potentials in the flux tubes is explained. Section 4 discusses polarity and intensity of field-aligned currents in parallel potentials. In Section 5, ionospheric injection scenario is summarized within the context of the coupling process of the magnetosphere and ionosphere.

2. Ionospheric injection

The ionospheric injection scenario proposed in Saka [2019] is as follows: (1) External electric fields penetrated in the polar ionosphere produce local accumulation/rarefaction of electric charges in the E-layer by the mobility difference of electrons and ions; (2) Resulting charge separation may be readily reduced by the secondary (polarization) electric fields; (3) A fraction of particle populations is released out of the ionosphere as ionospheric injections to sustain initial potential distributions in quasi-neutral equilibrium.

This ionospheric injection scenario is schematically shown in Figure 1. Ionospheric injection results in both generator and load. Localized westward electric fields ($\mathbf{E}_w$) accumulated negative charges (electrons) in lower latitudes leaving positive charges (ions) in higher latitudes because of differing electron and ion mobility in the E-layer (blue arrow, generator). Polarization electric fields ($\mathbf{E}_p$) produced by the charge separation moved ions to lower latitudes ($\mathbf{U}_{i\perp} = b_i \mathbf{E}_p$, b_i is mobility of ions) as Pedersen currents to neutralize the ionosphere (red arrow, load). To avoid a complete neutralization of the ionosphere, some positive charges (ions) in negative potential regions in lower latitudes and some negative charges (electrons) in positive potential regions in higher latitudes were expelled from the ionosphere. This partial neutralization process sustained original potential distributions in quasi-neutral equilibrium. In Figure 1, we do not include the Hall currents driven by the secondary polarization electric fields. The Hall current produce current vortices flowing

clockwise (as viewed from above) in a positive potential region in higher latitudes and counterclockwise in negative potentials in lower latitudes.

Meanwhile, geomagnetic field lines are not in equipotential equilibrium during ionospheric injections but instead develop both downward electric fields in positive potential regions of higher latitudes to extract electrons located there and upward electric fields in negative potential regions of lower latitudes to extract ions. **Ionospheric injection is an evaporation process of ionospheric electrons and ions along the flux tubes at the substorm onset.**

3. Development of parallel potentials

For about 10 minutes following Pi2 onset, nighttime magnetosphere could be in a transitional state repeating local field line dipolarization [Saka et al., 2010]. In this transitional interval, steady-state motions of electrons and ions can be assumed. In guiding center approximation, one-dimensional parallel motion could be given as,

$$v_{//}\frac{\partial v_{//}}{\partial s} = G_{//} + \frac{q|e|}{m_q}E_{//} - \frac{\mu_q}{m_q}\frac{\partial B}{\partial s} \qquad (1)$$

In equation (1), $|e|$ is the charge, m_q is the mass, μ_q is the magnetic moment, $G_{//}$ is the gravitational acceleration, B is the magnetic field strength, $E_{//}$ is the parallel electric field, $v_{//}$ is the parallel velocity, and s is along field lines. Note that $q=1$ for ions and $q=-1$ for electrons. In this equation, centrifugal force is ignored. Equation (1) can be reduced to the constants of the motion (W, μ),

$$W = \frac{m_q}{2}(v_{//}^2 + v_{\perp}^2) + q|e|\Phi \qquad (2)$$

$$\mu = \frac{m_q}{2B}v_{\perp}^2 \qquad (3)$$

Here, $v_{\perp}$ and Φ denote perpendicular velocity and electrostatic potential along the field lines, respectively.

Gravitational term in (1) can be ignored in (2) if the electrostatic potential above the ionosphere decreased below -10 Volt for ions.

Combination of equations (2) and (3) yields,

$$v_{//}^{'2} = v_{//}^2 + (1 - B'/B)v_{\perp}^2 + (2q|e|/m_q)(\Phi - \Phi') \qquad (4)$$

97 Equation (4) gives dynamical trajectory in phase space between two points, $(v_{//}^{'}, v_{\perp}^{'}; \Phi^{'})$

98 and $(v_{//}, v_{\perp}; \Phi)$, along the same field lines [e.g., Chiu and Schulz, 1978].

99 If the dynamical trajectory starts from the bottom-side ionosphere, $(v_{//}^{'}, v_{\perp}^{'}; \Phi^{'})$ is at the

100 ionospheric E-layer and $(v_{//}, v_{\perp}; \Phi)$ is either at 1,000km, 10,000 km, 20,000 km and at

101 geosynchronous (50,000 km) altitudes. The trajectory trace of the velocity space is shown in
102 Figures 2 and 3.
103 In Figure 2, both the magnetic mirror force and parallel potential accelerated ionospheric
104 sources. This acceleration process moved ionospheric source plasmas labelled (Σ) to the
105 bottom-right or to the bottom-left corner in velocity space as the altitudes increased from
106 1,000 km to the geosynchronous altitudes. Figure 2 illustrates two cases: (1) Ionospheric
107 electrons are accelerated in downward electric fields where field-aligned potential increased
108 with increasing altitudes; (2) Ionospheric ions are accelerated in upward electric fields where
109 the potential decreased with increasing altitudes. Assuming the Maxwell distribution function
110 for velocity distributions of ions and electrons above 1,000 km in altitudes, in accordance with
111 Liouville's theorem ($df/dt = 0$) we calculate parallel and perpendicular temperatures of
112 ionospheric species at altitudes of 1,000 km, 10,000 km, 20,000 km, and geosynchronous.
113 The velocity distribution function of ionospheric plasmas is given by,

114 $$f(v_{//}, v_{\perp}; \Phi) = \left(\frac{m_q}{2\pi k T_q}\right)^{3/2} \exp\left(\frac{m_q}{2kT_q}(v_{//}^2 + v_{\perp}^2) + \frac{q|e|\Phi}{kT_q}\right) \qquad (5)$$

115 Here kT_q is 1 eV for ions/electrons. Electrostatic potential Φ is 0 volt at the ionosphere.

116 The temperature of parallel/perpendicular component in eV is given by $\frac{m_q}{2}\left\langle v_{//,\perp}^2 \right\rangle$, where

117 $$\left\langle v_{//,\perp}^2 \right\rangle = \frac{\int_{\Sigma} v_{//,\perp}^2 \, f(v) d^3 v}{\int_{\Sigma} f(v) d^3 v} \qquad (6)$$

118 **Integration was carried out over the velocity space (Σ) bounded by the hyperbolic**

119 **curves, both in negative (earthward) and positive (tailward) velocity component in $v_{//}$.**

120 For both ions and electrons, parallel and perpendicular temperatures $\left(\frac{m_q}{2}\left\langle v_{//}^2 \right\rangle, \frac{m_q}{2}\left\langle v_{\perp}^2 \right\rangle\right)$

initially (0.5 eV, 1.0 eV) in the ionosphere changed to (11.3 eV, 0.70 eV) at 1,000 km where electrostatic potential was 10 V for electrons and -10 V for ions. Temperatures changed to (51.9 eV, 0.09 eV) at 10,000 km where electrostatic potential was 50 V for electrons and -50 V for ions. When electrostatic potential further increased to 200 V for electrons and decreased to -200 V for ions at 20,000 km, temperatures changed to (202.0 eV, 0.02 eV). At geosynchronous altitudes, temperatures changed to (502 eV, 0.002 eV) where potential is assumed to be 500 V for electrons and -500 V for ions. Parallel potential and mirror geometry skewed velocity space of the ionospheric source and increased parallel temperatures and decreased perpendicular ones at altitudes above the ionosphere.

The other cases where parallel potentials act as a potential barrier are shown in Figure 3. In this type, dynamical trajectories filled all velocity space in $v_{//}$, and parallel temperature (0.5 eV at the ionosphere) did not change above the ionosphere up to geosynchronous altitudes, while perpendicular temperature decreased to 0.87 eV at 20,000 km, and to 0.42 eV at geosynchronous altitudes. We conclude that accelerating potential raised parallel temperature of the escaping ionospheric species. The potential barriers did not change the parallel temperature of the ionospheric source.

A brief explanation is given below as to how the local potentials that have extracted electrons and ions from the ionosphere developed at higher altitudes above the ionosphere. We note that electrons and ions traveling earthward in the left-hand side of the velocity space marked by Σ may contribute to the development of parallel potentials. In flux tubes where parallel potential accelerates electrons (ions) out of the ionosphere, the same parallel potential in the flux tubes acts as a potential barrier for ions (electrons) escaping ionosphere. In this flux tube small pitch-angle electrons (ions) and large pitch-angle ions (electrons) traveling earthward generate downward (upward) electric fields by charge separation along the flux tubes of mirror geometry [Alfven and Falthammar, 1963; Persson, 1963; Stern, 1981]. These potentials are global in scale and vary monotonically from ionosphere to the equator. However, a rate of parallel potential change (parallel electric fields) may decrease above an altitude of 10,000 km because magnetic mirror force drops rapidly in these regions.

The resultant potential distributions in the polar ionosphere and in the magnetosphere are presented in Figure 4. Because of parallel potentials in the magnetosphere, potential difference in the ionosphere never weakens but instead amplifies during equatorial projection.

4. Field-aligned current

Ions in the E layer drifted from positive potentials in higher latitudes to negative potentials in lower latitudes to discharge imbalance produced by the mobility difference. Drift velocities of these ions ($\mathbf{U}_{i\perp}$) may be given as,

$$\mathbf{u}_{i\perp} = \frac{\Omega_i}{B\nu_{in}}\mathbf{E}_p \qquad (7)$$

Here, Ω_i , ν_{in} , $\mathbf{E}_p$ denote ion cyclotron frequency, ion-neutral collision frequency and secondary polarization electric fields, respectively. Substituting mean ion cyclotron and ion-neutral collision frequencies in (7), we have ion drift velocities on the order of 5.9 x 10^1 m/s for electric fields of the order of 0.1 V/m. Those drifting ions carry southward Pedersen currents of the order of $1.0\mu A/m^2$ in the E-layer. **These ionospheric currents might be redirected to the field-aligned currents at the poleward and equatorward edge of the flow channel of the current to close 2-D current system. We therefore suggest that field-aligned currents of the order of $1.0\mu A/m^2$ may flow above the ionosphere in the ionospheric injection scenario. To test this hypothesis, we calculate the field-aligned currents along the dynamical trajectories using $\mathbf{J}_{//q} = nq|e|\langle v_{//}\rangle$, where**

$$\langle v_{//}\rangle = \frac{\int_\Sigma v_{//}\, f(v) d^3v}{\int_\Sigma f(v) d^3v} \qquad \textbf{(8)}$$

To calculate electric currents, velocity space integration was carried out only in the positive velocity component in $v_{//}$ (traveling tailward), because those in negative velocity component traveling earthward may be reflected in the magnetic mirror geometry and cancel the earthward currents. The results show that ionospheric electrons at altitudes of 10,000 km (electrostatic potential is 50 V) carry downward field-aligned currents of the order of $2.0\mu A/m^2$ at the number density $10^1/m^3$. This is a fraction of the background density at those altitudes ($n = 10^9/m^3$). We conclude that upward flowing ionospheric electrons may close Pedersen currents at the poleward edge of the channel, while upward flowing ionospheric ions (oxygen ions) at the equatorward edge of the channel carried $0.69nA/m^2$ at the same altitudes

(electrostatic potential is -50 V) and same number density of electron currents. Electric currents carried by the ions are smaller than those carried by electrons by the mass ratio of electrons and ions if temperatures of electrons and ions are the same. They cannot provide sufficient current density to close the Pedersen currents. Therefore, electrons from the magnetosphere are necessary for closing the Pedersen currents at the equatorward edge of the channel.

5. Summary and Discussion

Despite the ionospheric dynamo processes driven by the neutral wind, local electrostatic fields that form in less than one minute may be expected in ionospheric injection because electrons participate the dynamo process. Electrons are pumped up towards negative electrodes in lower latitudes by ExB drift. The drift generates poleward Hall currents flowing in an opposite direction in the equatorward electric field. The westward electric fields of the magnetospheric origin may generate the ionospheric dynamo. The dynamo process yielded plasma injections arising out of the ionosphere (evaporation of ionospheric plasmas) and generated preferentially field-aligned potentials below 10,000 km.

Although the substorm onset would be triggered initially by the magnetospheric convection enhancement (arrival of the Dipolarization Front from the tail), we suggest that activation of the ionospheric dynamo (auroral onset) may be controlled by the intensity of westward electric fields penetrating the auroral ionosphere. Because electric fields penetrating the ionosphere are stronger in dark hemisphere (lower Pedersen conductance) than in sunlit hemisphere (higher Pedersen conductance) [Saka, 2019], auroras are more active in the dark hemisphere [Newell et al., 1996].

Field-aligned potentials were generated in the magnetosphere such that the ionospheric potentials were amplified during their equatorial projection. This means that the ionosphere responded to the initial dipolarization by returning the southward electric fields to the dipolarization region in the magnetosphere. The southward electric fields in the ionosphere that became earthward electric fields in the plasma sheet further displaced the dipolarizing flux tube eastward which relaxed the radial inhomogeneity and intensified the dipolarization [Saka, 2020]. This positive feedback loop may happen in the magnetosphere and ionosphere systems with asymmetric development of the dipolarization region in dawn-dusk directions. This asymmetry may be related to the difference in onset time of substorm current wedge in dawn and dusk sectors [Nagai, 1991]. In this scenario, Harang Discontinuity (HD) is generated in the auroral ionosphere through the ionospheric injection processes and projected

back to the magnetosphere to modify the existing magnetospheric convection patterns [e.g., Artemyev et al., 2016]. This scenario differs from the proposal of [Erickson et al., 1991; Liu and Rostoker, 1991] that asymmetric plasma pressure distribution introduced in the equatorial plane of the nightside magnetosphere produced HD in the polar ionosphere.

It was suggested that a deformation velocity of aurora is about 5-8 km/s regardless of its scale size [Oguti, 1975a, 1975b]. Oguti [1975b] noted from his observations that large-sale auroras (~ 1000 km) such as bulge or surge are the sum of small-scale auroras (~3 km) such as rays. Small-scale auroras that may be equivalent to the minimum size of the electrostatic potential of negative charge are fundamental to the MI coupling processes in the ionospheric injection scenario.

6. Data availability. No data sets were use in this article.

7. Competing interest. The author declares that there is no conflict of interest.

References

Alfven, H. and Falthammar, C.-G.: Cosmical Electrodynamics, 2nd ed., Oxford University Press, New York, 1963.

Artemyev, A.V., Angelopoulos, A., Runov, A., and Zelenyi, L.M.: Earthward electric field and its reversal in the near-Earth current sheet, J. Geophys. Res., 121, 10803-10812, doi:10.1002/2016JA023200, 2016.

Baker, D.N., Pulkkinen, T.I., Angelopoulos, V., Baumjohann, W., and McPherron, R.L.: Neutral line model of substorms: Past results and present view, J. Geophys. Res., 101, 12795-130010, 1996.

Birn, J., Hesse, M., Haerendel, G., Baumjohann, W., and Shiokawa, K: Flow braking and the substorm current wedge, Geophys. Res., 104, 19895-19903, 1999.

Birn, J., Raeder, J., Wang, Y.L., Wolf, R.A., and Hesse, M.: On the propagation of bubbles in the geomagnetic tail, Ann. Geophys., 22, 1773-1786, 2004.

Chiu, Y.T. and Schulz, M.: Self-consistent particle and parallel electrostatic field distributions in the magnetospheric-ionospheric auroral region, J. Geophys. Res. 83, 629-642, 1978.

253 Erickson, G.M., Spiro, R.W., and Wolf, R.A.: The physics of the Harang discontinuity, J.
254 Geophys. Res., 96, 1633-1645, 1991.
255 Liu, W.W., and Rostoker, G.: Effects of dawn-dusk pressure asymmetry on convection in the
256 central plasma sheet, J. Geophys. Res., 96, 11501-11512, 1991.
257 Liu, W.W., and Liang, J.: Disruption of magnetospheric current sheet by quasi-electrostatic
258 field, Ann. Geophys., 27, 1941-1950, 2009.
259 Liu, J., Angelopoulos, V., Zhou, X.-Z., and Runov, A.: Magnetic flux transport by dipolarizing
260 flux bundles, J. Geophys. Res., 119, 909-926, doi:10.1002/2013JA019395, 2014.
261 Lui, A.T.Y.: Current disruption in the Earth's magnetosphere: Observations and models, J.
262 Geophys. Res., 101, 13067-13088, 1996.
263 McPherron, R.L., Russell, C.T., and Aubry, M.P.: Satellite studies of magnetospheric
264 substorms on August 15, 1968: 9. Phenomenological model for substorms, J.
265 Geophys. Res., 78, 3131-3148, 1973.
266 Nagai, T.: An empirical model of substorm-related magnetic field variations at synchronous
267 orbit, Magnetospheric substorms, Geophysical monograph 64, Edited by J.R. Kan,
268 T.A. Potemra, S. Kokubun, and T. Iijima, 91-95, 1991.
269 Newell, P.T., Meng, C.I., and Lyons, K.M.: Suppression of discrete aurorae by sunlight,
270 Nature, 381, 766-767, 1996.
271 Nielsen, E., and Greenwald, R.A.: Variations in ionospheric currents and electric fields in
272 association with absorption spikes during substorm expansion phase, J. Geophys.
273 Res., 83, 5645-5654, 1978.
274 Oguti, T.: Similarity between global auroral deformations in DAPP photographs and small
275 scale deformations observed by a TV camera, J. Atmos. Terr. Phys., 37, 1413-1418,
276 1975a.
277 Oguti, T.: Metamorphoses of aurora, Memoirs of NIPR, series A, 12, 1975b.
278 Persson, H.: Electric field along a magnetic line of force in a low-density plasma: Phys. Fluids,
279 6, 1756-1759, 1963.
280 Runov, A., Angelopoulos, V., Zhou, X.-Z., Zhang, X.-J., Li, S., Plaschke, F., and Bonnell, J.:
281 A THEMIS multicase study of dipolarization fronts in the magnetotail plasma sheet, J.
282 Geophys. Res., 116, A05216, doi:10.1029/2010JA016316, 2011.
283 Roux, A., Perraut, S., Robert, P., Morane, A., Pedersen, A., Korth, A., Kremser, G., Aparicio,
284 B., Rodgers, D., and Pellinen, R.: Plasma sheet instability related to the westward
285 traveling surge, J. Geophys. Res., 96, 17697-17714, 1991.
286 Saka, O., Hayashi, K, and Thomsen, M.: First 10 min intervals of Pi2 onset at
287 geosynchronous altitudes during the expansion of energetic ion regions in the
288 nighttime sector, J. Atmos. Solar Terr. Phys., 72, 1100-1109, 2010.

Saka, O.: A new scenario applying traffic flow analogy to poleward expansion of auroras, Ann. Geophys., 37, 381-387, 2019.

Saka, O.: The increase in the curvature radius of geomagnetic field lines preceding a classical dipolarization, Ann. Geophys., 38, 467-479, 2020.

Stern, D.P.: One-dimensional models of quasi-neutral parallel electric fields, J. Geophys. Res., 86, 5839-5860, 1981.

Tanaka, T., Nakamizo, A., Yoshikawa, A., Fujita, S., Shinagawa, H., Shimazu, H., Kikuchi, T., and Hashimoto, K.: Substorm convection and current system deduced from the global simulation, J. Geophys. Res., 115, A05220, doi:10.1029/2009JA014676, 2010.

Wahlund, J.-E., Opgenoorth, H.J., Haggstrom, I., Winser, K.J., and Jones, G.O.: EISCAT observations of topside ionospheric outflows during auroral activity: revisited, J.Geophys.Res., 97, 3019-3017, 1992.

Figure captions

Figure 1.

A schematic illustration of the plasma injection arising out of dynamic ionosphere (ionospheric injection). See text for detailed explanation.

Figure 2.

Regions of velocity space (Σ) occupied by the ionospheric species are shown. They were accelerated by the parallel potentials and magnetic mirror force: (A) electrons (ions) at 1,000 km altitudes for parallel potentials of 10 V (-10 V), (B) electrons (ions) at 10,000 km for 50 V (-50 V), (C) electrons (ions) at 20,000 km for 200 V (-200 V), and (D) electrons (ions) at geosynchronous altitudes for 500 V (-500 V). In the velocity space, ($v_{//}$, $v_{\perp}$) are normalized by the thermal velocity of respective particles (1 eV for this case).

Figure 3.

Same as Figure 2 but parallel potential behaved as potential barriers: (A) electrons (ions) at 1,000 km for parallel potentials of -10 V (10 V), (B) electrons (ions) at 10,000 km for -50 V (50 V), (C) electrons (ions) at 20,000 km for -200 V (200 V), and (D) electrons (ions) at

geosynchronous altitudes for -500 V (500 V).

Figure 4.

Equatorial projection of the ionospheric potentials (ϕ_i^+ and ϕ_i^-) from southern and northern hemispheres is illustrated. Ionospheric potentials are positive in higher latitudes (ϕ_i^+) and negative in lower latitudes (ϕ_i^-). Field-aligned potential amplified potential difference in the ionosphere during the equatorial projection ($\phi_m^{++} > \phi_i^+$, $\phi_m^{--} < \phi_i^-$). Earthward electric fields are produced in the plasma sheet.

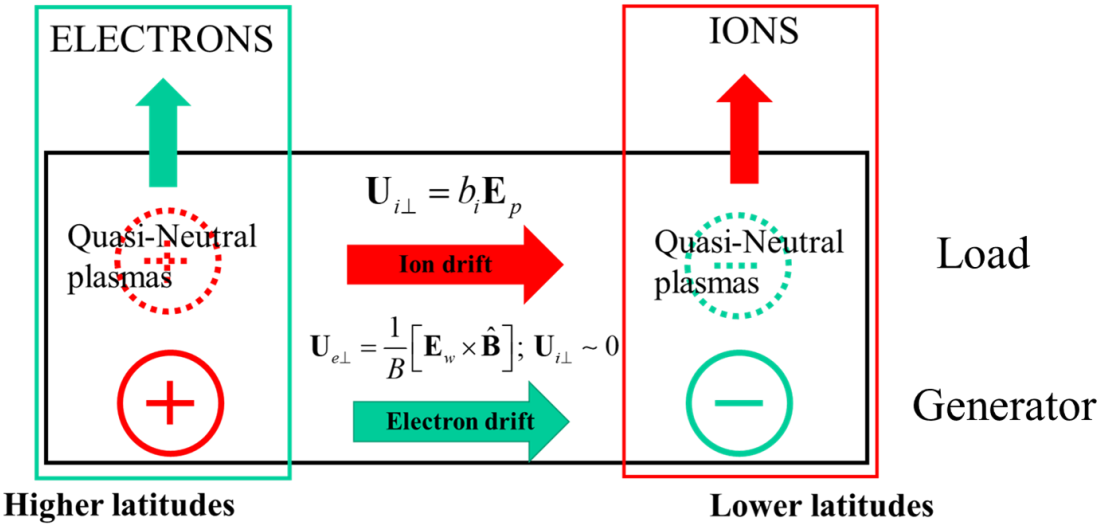
ELECTRONS
IONS
Quasi-Neutral plasmas
Quasi-Neutral plasmas
$\mathbf{U}_{i\perp} = b_i \mathbf{E}_p$
Ion drift
$\mathbf{U}_{e\perp} = \frac{1}{B}\left[\mathbf{E}_w \times \hat{\mathbf{B}}\right]; \mathbf{U}_{i\perp} \sim 0$
Electron drift
Load
Generator
Higher latitudes
Lower latitudes

Figure 1

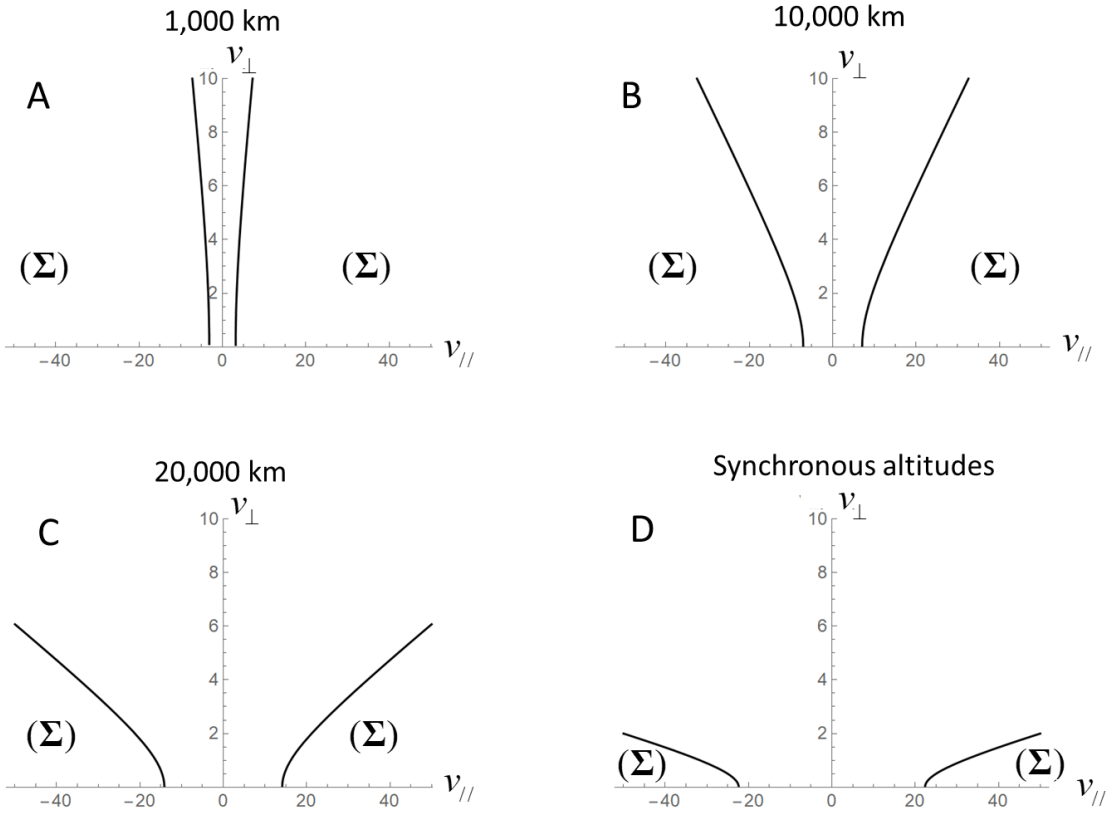
1,000 km
A
$v_\perp$
(Σ)
(Σ)
$v_{//}$
10,000 km
B
$v_\perp$
(Σ)
(Σ)
$v_{//}$
20,000 km
C
$v_\perp$
(Σ)
(Σ)
$v_{//}$
Synchronous altitudes
D
$v_\perp$
(Σ)
(Σ)
$v_{//}$

Figure 2

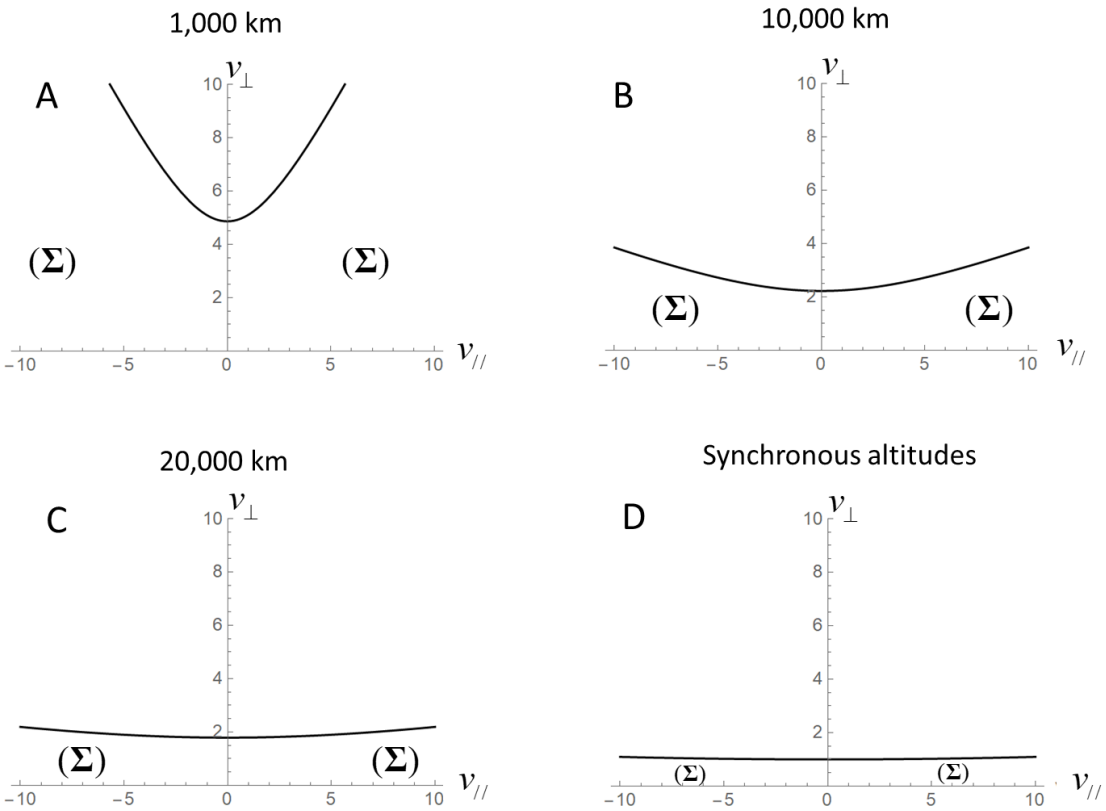
1,000 km
A
$v_\perp$
$v_{//}$
(Σ)
(Σ)
10,000 km
B
20,000 km
C
Synchronous altitudes
D

Figure 3

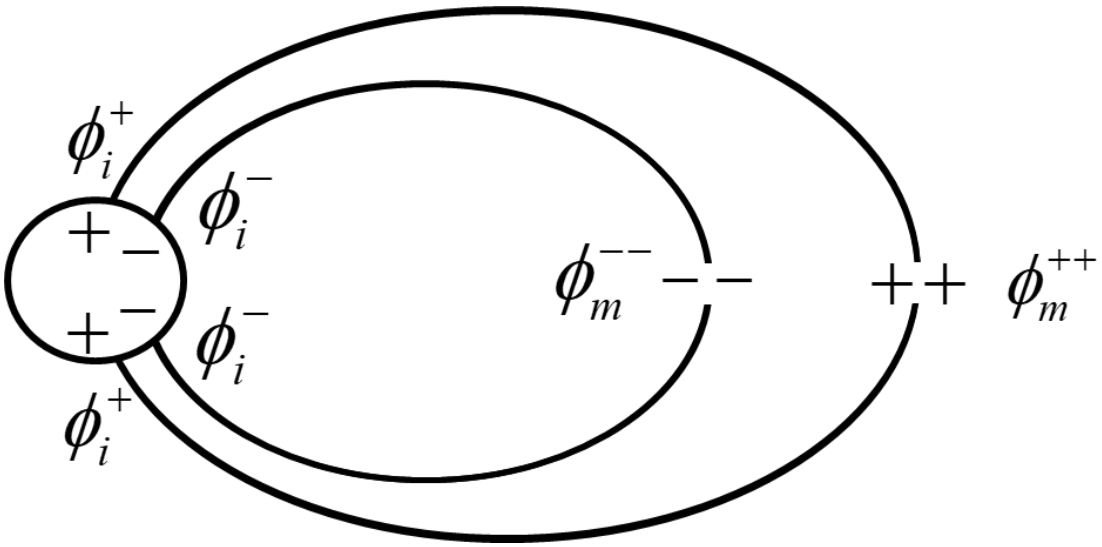

Figure 4

333